HHS Public Access

Author manuscript

Lab Chip. Author manuscript; available in PMC 2020 August 10.

Published in final edited form as:

Lab Chip. 2019 July 21; 19(14): 2415–2424. doi:10.1039/c9lc00438f.

Ultra-compact, automated microdroplet radiosynthesizer

Jia Wang[1,2], **Philip H. Chao**[1,2], **R. Michael van Dam**[1,2,*]

[1]Crump Institute for Molecular Imaging and Department of Molecular & Medical Pharmacology, David Geffen School of Medicine, University of California at Los Angeles (UCLA), Los Angeles, CA, USA

[2]Department of Bioengineering, UCLA, Los Angeles, CA, USA

Abstract

Application of microfluidics offers numerous advantages in the field of radiochemistry and could enable dramatic reductions in the cost of producing radiotracers for positron emission tomography (PET). Droplet-based microfluidics, in particular, requires only microgram quantities of expensive precursors and reagents (compared to mg used in conventional radiochemistry systems), and occupies a more compact footprint (potentially eliminating the need for specialized shielding facilities, i.e. hot cells). However, the reported platforms for droplet radiosynthesis have several drawbacks, including high cost/complexity of microfluidic reactors, requirement for manual intervention (e.g. for adding reagents), or difficulty in precise control of droplet processes. We describe here a platform based on a particularly simple chip, where reactions take place atop a hydrophobic substrate patterned with a circular hydrophilic liquid trap. The overall supporting hardware (heater, rotating carousel of reagent dispensers, etc.) is very simple and the whole system could be packaged into a very compact format (about the size of a coffee cup). We demonstrate the consistent synthesis of [^{18}F]fallypride with high yield, and show that protocols optimized using a high-throughput optimization platform we have developed can be readily translated to this device with no changes or re-optimization. We are currently exploring the use of this platform for routine production of a variety of ^{18}F-labeled tracers for preclinical imaging and for production of tracers in clinically-relevant amounts by integrating the system with an upstream radionuclide concentrator.

Keywords

Droplet synthesis; Organic synthesis; Microfluidics; Radiochemistry; Molecular imaging

1 Introduction

Positron emission tomography (PET) is a non-invasive medical imaging method that can be used as a research tool for studying the biological processes involved in the course of

*Corresponding author: mvandam@mednet.ucla.edu.

6 Author contributions

J.W. and R.M.V. designed the microdroplet radiosynthesizer. P.H.C. assisted with parts machining and provided input for control system design. J.W. and R.M.V. designed experiments. J.W. assembled the system, performed experiments and analyzed results and data. J.W. and R.M.V. wrote the manuscript with input from P.H.C..

diseases and making critical measurements during the development of new drugs [1–3]. It is also widely used in the clinic to diagnose and stage disease, predict treatment response, and evaluate efficacy of treatment [4–6]; furthermore, PET can also be used to help guide treatment and serves a critical role in the emerging field of personalized medicine [7]. Shortly before undergoing a PET imaging procedure, the patient (or subject) must be injected with a short-lived radiolabeled compound, which is designed to highlight a particular biological target or pathway.

The current processes and technologies for producing these PET "tracers" are complex and expensive, which greatly hinders research efforts into the development and validation of novel tracers, or the translation of new tracers into the clinic. For more than a decade, investigators have been exploring the use of microfluidics to improve the production of PET tracers [8–10] and have advanced this technology to the point of demonstrating production of tracers suitable for clinical use [11–13].

These studies, especially the use of micro-volume reactors [13–17] or droplet-based reactors [18–20], have revealed several important advantages of microfluidics in radiochemistry that can reduce the cost and complexity of PET tracer production [21]. Though all uses of PET tracers can benefit, the improvements will be especially impactful for the small batches needed in research applications or in the initial studies to develop novel tracers and translate them to the clinic. Particularly important advantages of small-volume radiosynthesizers compared to conventional synthesizers are the significant reduction in footprint of the radiochemistry setup, enabling self-shielding rather than requiring operation within specialized "hot cells", and the 2–3 orders of magnitude reduction in consumption of expensive reagents (e.g. precursors, peptides, etc.). Small-volume synthesis has also been shown to boost the molar activity of tracers produced via isotope exchange [22] and can achieve high molar activities even when producing small batches of tracers [23], both of which are not possible in conventional systems unless very high amounts of radioactivity are used.

As a testament to the versatility of droplet-based approaches, a wide range of PET tracers have been synthesized using these methods[24], including [^{18}F]fallypride [15,20,25,26], [^{18}F]FDG [14,20,24,27,28], [^{18}F]FLT [29], [^{18}F]SFB [24,30], [^{18}F]FDOPA [31], sulfonyl [^{18}F]fluoride [19], [^{18}F]FMISO [16], [^{18}F]FES [16], [^{18}F]AMBF$_3$-TATE [22], etc. In addition, these microscale reactors are scalable, with the possibility to produce clinically-relevant doses by increasing the concentration of radioisotope supplied into the system [13,32,33].

Our group has focused particularly on droplet-radiochemistry platforms, including electrowetting-on-dielectric (EWOD) devices [18] and a more recent system using patterned wettability for passive droplet transport [20], due to the extremely small reaction volumes and straightforward fluidic system. In the passive transport approach, the chip consists of a Teflon coated silicon wafer with patterned circular hydrophilic reaction zone in the center and several radial tapered channels to transport droplets from reagent loading sites at the periphery into the reaction zone. Though this approach significantly decreased the chip cost and complexity, and we could successfully synthesize [^{18}F]fallypride and [^{18}F]FDG, we have found the behavior of the droplets to be sensitive to the solvent type, temperature, and volume, sometimes leading to unwanted spreading out of the solution along the tapered

reagent pathways of the chip. Such spreading can adversely affect synthesis performance and lead to inconsistent results, requiring expenditure of time and effort to optimize reagents and solvents, loading protocols (timing) and other aspects to achieve high synthesis performance.

To avoid those issues, and further streamline the adoption of new protocols to the microdroplet format, we present here an even simpler microfluidic chip with just a circular hydrophilic reaction zone. Instead of reagents moving from multiple fixed loading sites (located under reagent dispensers) to the reaction zone spontaneously, a simple system is designed to rotate the chip under a carousel of reagent dispensers for on-demand loading of desired reagents when needed. This change was found to significantly improve the performance of the on-chip reaction, and the amount of the reaction product that could be collected from the chip. We also spent considerable effort in designing the system to be as compact as possible (similar to the size of a coffee cup), demonstrating that sophisticated multi-step radiochemistry can be accomplished with a very small apparatus. The compact size (10 × 6 × 12 cm; W x D x H), which includes the reagent handling system, microreactor, and temperature control system, is a tremendous advantage in radiochemistry facilities where shielded space is at a premium. For example, multiple droplet synthesizers could be operated inside a single hot cell, or the droplet synthesizer could be operated outside the hot cell by adding localized shielding. Though the system currently requires external systems for purification and formulation, the overall setup is significantly smaller than other radiosynthesizers. To give a clearer overall context for our current work, the features of various radiosynthesizer technologies (including conventional systems and microscale systems) are compared in Table 1.

In this paper, we present the design and operation of this next-generation microdroplet radiosynthesizer and show that it can quickly and efficiently synthesize the PET tracer [^{18}F]fallypride. As shown in Table 1, it can be seen that this system enables the highest radiochemical yield (RCY), shortest synthesis time, and lowest amount of precursor compared to various other systems used for the synthesis of this tracer. Furthermore, the platform is able to leverage our other efforts to develop high-throughput radiochemistry methods (i.e. using arrays of hydrophilic reaction zones on a single chip) [34], enabling the rapid translation of the optimum protocol to the new automated platform with zero changes. As a result of the simplified approach, we expect to help enable the low-cost production of diverse tracers for research as well as clinical applications.

2 Materials and Methods

2.1 Materials

Anhydrous acetonitrile (MeCN, 99.8%), methanol (MeOH), 2,3-dimethyl-2-butanol (thexyl alcohol, 98%), trimethylamine (TEA), ammonium formate (NH_4HCO_2; 97%) were purchased from Sigma-Aldrich. Tetrabutylammounium bicarbonate ($TBAHCO_3$, 75mM), tosyl fallypride (fallypride precursor, >90%) and fallypride (reference standard for [^{18}F]fallypride, >95%) were purchased from ABX Advanced Biochemical Compounds (Radeberg, Germany). Food dye was purchased from Kroger (Cincinnati, OH, USA) and diluted with solvents in the ratio of 1:100 (v/v) to perform a mock synthesis. DI water was

obtained from a Milli-Q water purification system (EMD Millipore Corporation, Berlin, Germany). No-carrier-added [^{18}F]fluoride in [^{18}O]H_2O was obtained from the UCLA Ahmanson Biomedical Cyclotron Facility.

2.2 Apparatus

Reactions were performed on microfluidic chips (Figure 1), each comprising a hydrophilic circular reaction site (4 mm diameter) patterned in the hydrophobic Teflon AF surface of a silicon chip (25 mm x 27.5 mm). The patterned chips were prepared by coating silicon wafers with Teflon AF, and then etching away the coating to leave the desired hydrophilic pattern as described previously [20]. For this work, we omitted the final Piranha cleaning step. Chips were used once each and then discarded after use.

Operations on the microfluidic chip were automated by a custom-built compact framework (Figure 2), consisting of a rotating, temperature-controlled platform, a set of reagent dispensers, and a collection system to remove the reaction droplet at the end of the synthesis. The control system is shown in Figure 3.

Heating was provided by placing the chip in direct contact with a 25 mm x 25 mm ceramic heater (Ultramic CER-1–01-00093, Watlow, St. Louis, MO, USA). A thin layer of thermal conducting paste (OT-201–2, OMEGA, Norwalk, CT, USA) was applied between the chip and heater to improve heat transfer. The chips could easily be aligned during installation by lining up three edges of the chip with the edges of the heater. The heater was glued atop a 40 mm x 40 mm thermoelectric device (Peltier, VT-199–1.4–0.8, TE Technology, Traverse City, MI, USA) mounted to a 52 mm x 52 mm integrated heatsink and fan (4–202004UA76153, Cool Innovations, Concord, Canada). The integrated cooling part was mounted via a custom aluminum plate to a motorized rotation stage (OSMS-40YAW, OptoSigma, Santa Ana, CA, USA). The signal from a K-type thermocouple embedded in the heater was amplified through a K-type thermocouple amplifier (AD595CQ, Analog Devices, Norwood, MA, USA) and connected to an analog input of the data acquisition device (DAQ; NI USB-6003, National Instruments, Austin, TX, USA). The power supply (120 V AC) for the heater was controlled by a solid-state relay (SSR, Model 120D25, Opto 22, Temecula, CA, USA) driven by a digital output of the DAQ. An on-off temperature controller was programmed in LabView (National Instruments) to maintain a desired setpoint. A power step down module (2596 SDC, Model 180057, DROK, Guangzhou, China) was connected to a 24V power supply to provide 12V for the cooling fan, which was switched on during cooling via an electromechanical relay (EMR, SRD-05VDC-SL-C, Songle Relay, Yuyao city, Zhejiang, China) controlled by the LabView program. The motorized stage was driven by a stage controller (GSC-01, OptoSigma) controlled by the LabView through serial communication.

Droplets were loaded at the reaction site of the microfluidic chip through miniature, solenoid-based, non-contact dispensers. Chemically-inert dispensers with FFKM seal (INKX0514100A, Lee Company, Westbrook, CT, USA) were used for reagents containing organic solvents, while a dispenser with EPDM seal (INKX0514300A, Lee Company) was utilized to dispense [^{18}F]fluoride solution. Each dispenser was connected to a pressurized vial of a reagent and the internal solenoid valve was opened momentarily to dispense liquid. More details of the fluidic connections were reported previously [20]. Each dispenser was

connected to a dedicated controller (IECX0501350A, Lee Company), driven by a digital output from the DAQ and controlled via the LabView program. Since the volume of dispensed liquid is related to the driving pressure, the opening duration of the valve, and physical properties (e.g. viscosity) of the solvent, calibration curves were generated for each reagent as described previously [20].

A fixture was built to hold up to 7 dispensers with nozzles located ~3 mm above the chip. Each dispenser was secured within a hole by an O-ring (ORBN005, Buna-N size 005, Sur-Seal Corporation, Cincinnati, OH, USA). The fixture was mounted to a vertically-oriented movable slide, and a single-acting air cylinder (6604K13, McMaster-Carr) was configured to allow the fixture to be raised 16 mm above the surface to facilitate installation and removal of microfluidic chips and cleaning of the dispensers. The air cylinder was connected to a 3-way valve (LVM105R-2, SMC Corporation) to apply either pressure (~210 kPa [~30 psi]) or vent to atmosphere, and the valve was controlled by the LabView program.

The heater and chip were mounted off-center of the rotation axis. During multi-step reactions, the chip was rotated to position the reaction site underneath a dispenser to add the desired reagent, and was then rotated to a position in between dispensers while performing evaporations or reactions at elevated temperatures.

To transfer the final crude product from the reaction site on the chip to the collection vial, a metal tubing (0.25 mm inner diameter) was mounted in the dispenser fixture such that the end was ~0.5 mm above the chip surface. At the end of synthesis, the platform was rotated such that the reaction droplet was aligned under the collection tube and vacuum was applied to the headspace of the collection vial using a compact vacuum pump (0–16” Hg vacuum range, D2028, Airpon, Ningbo, China) connected via a vacuum regulator (ITV0090–3UBL, SMC Corporation) controlled via LabView program. Vacuum pressure was ramped from 0 to 14 kPa (~2 psi, 0.01 psi increment every 50 ms) over 10 s to transfer the droplet into the vial.

After the synthesis, dispensers were each cleaned by flushing with DI water (1 mL) and MeOH (1 mL) in sequence, driven at 69 kPa [~10 psi], and then drying with nitrogen for 2 min. The used chip was removed with tweezers and discarded.

2.3 Automated droplet synthesis of [^{18}F]fallypride

As a model reaction to demonstrate the ability to perform multi-step reactions automatically with the microdroplet radiosynthesizer, we performed syntheses of the PET tracer [^{18}F]fallypride. The synthesis protocol was adapted from a manual synthesis protocol developed via manual optimization efforts using microfluidic chips having a similar circular hydrophilic reaction zone[34].

A [^{18}F]fluoride stock solution was prepared by mixing [^{18}F]fluoride/[^{18}O]H_2O (60 μL, ~110 MBq [~3 mCi]) with 75 mM $TBAHCO_3$ solution (40 μL). The final $TBAHCO_3$ concentration was 30 mM. Precursor stock solution was prepared by dissolving tosyl-fallypride precursor (2 mg) in a mixture of MeCN and thexyl alcohol (1:1 v/v, 100 μL) to result in a final concentration of 39 mM. A stock solution for dilution of the crude product

prior to collection was prepared from a mixture of MeOH and DI water (9:1, v/v, 500 μL). These solutions were loaded into individual reagent vials connected to dispensers.

To carry out the synthesis on the chip, the chip was first rotated to position the reaction site below the [^{18}F]fluoride/TBAHCO$_3$ dispenser and eight 1 μL droplets of [^{18}F]fluoride/TBAHCO$_3$ solution (~8.9 MBq; ~0.24 mCi) were sequentially loaded onto the chip (total time < 10s). The chip was rotated 45° counterclockwise (CCW) and heated to 105°C for 1 min to evaporate the solvent and leave a dried residue of the [^{18}F]TBAF complex at the reaction site. Then, the chip was rotated 45° CCW to position the reaction site under the precursor dispenser and twelve 0.5 μL droplets of precursor solution were loaded to dissolve the dried residue. Next, the chip was rotated 45° CCW and heated to 110°C for 7 min to perform the radiofluorination reaction. Afterwards, the chip was rotated 45° CCW to position the reaction site under the collection solution dispenser, and twenty 1 μL droplets of collection solution were deposited to dilute the crude product. After rotating the chip 90° CCW to position the reaction site under the collection tube, the diluted solution was transferred into the collection vial by applying vacuum. The collection process was repeated a total of four times to minimize the residue on the chip (i.e. by rotating the chip 90° CW back to the collection solution dispenser, loading more collection solution, etc.). A schematic of the whole synthesis process is shown in Figure 4.

To compare the performance of the new setup to our previous work, the same [^{18}F]fallypride synthesis conditions were implemented on our previous “passive transport” chip. The chip was composed of one hydrophilic 4 mm reaction site and six radial, tapered, hydrophilic fluid delivery ”channels” (Figure 5B), and reagent delivery and production collection were performed as previously described [20].

2.4 Analytical methods

Performance of the [^{18}F]fallypride synthesis on the chip was assessed through measurements of radioactivity and fluorination efficiency.

Radioactivity was measured with a calibrated dose calibrator (CRC-25R) at various times throughout the synthesis process, including starting radioactivity on the chip after loading of [^{18}F]fluoride/TBAHCO$_3$ stock solution, radioactivity of crude product transferred into the collection vial and radioactivity of residue on the chip after collection step. Radioactivity recovery was calculated as the ratio of radioactivity of collected crude product to starting radioactivity on the chip. Residual activity on the chip was the ratio of radioactivity on the chip after collection to the starting radioactivity on the chip. All measurements were corrected for decay.

Fluorination efficiency of the crude product collected from the chip was determined via radio thin layer chromatography (radio-TLC). A 1 μL droplet was spotted on a silica gel 60 F_{254} sheets (aluminum backing) with a micropipette. The TLC plate was dried in air and developed in the mobile phase of 60% MeCN in 25 mM NH_4HCO_2 with 1% TEA (v/v), and then analyzed with a scanner (MiniGITA star, Raytest, Straubenhardt, Germany). The resulting chromatograms showed peaks corresponding to unreacted [^{18}F]fluoride (R_f=0.0) and [^{18}F]fallypride (R_f=0.9). Fluorination efficiency was calculated as the peak area of the

[^{18}F]fallypride peak divided by the area of both peaks. Crude radiochemical yield (crude RCY, decay-corrected) was defined as the radioactivity recovery times the fluorination efficiency.

In some cases, radio-HPLC purification of the collected crude product was carried out using a Smartline HPLC system (Knauer, Berlin, Germany) equipped with a degasser (Model 5050), pump (Model 1000), a UV (254nm) detector (Eckert & Ziegler, Berlin, Germany) and a gamma-radiation detector and counter (B-FC-4100 and BFC-1000; Bioscan, Inc., Poway, CA, USA). Separation was performed using an analytical C18 column (Kinetex, 250 × 4.6 mm, 5 μm, Phenomenex) with mobile phase (60% MeCN in 25 mM NH_4HCO_2 with 1% TEA (v/v)) at 1.5 mL/min flow rate. The crude product collected from the chip was injected into the HPLC system, and the [^{18}F]fallypride fraction (~2 mL) was collected (retention time ~4.5 min). Chromatograms were recorded using a GinaStar analog-to-digital converter (raytest USA, Inc., Wilmington, NC, USA) and GinaStar software (raytest USA, Inc.) running on a PC. The collected product fraction was then dried by evaporation of solvent in an oil bath at 110°C for 8 min with nitrogen flow, and then redissolved in PBS. The purity and identity of the purified [^{18}F]fallypride was verified using the same HPLC system and conditions.

For the experiments that included the purification step, the radioactivity of purified product recovered from HPLC was also measured. The purification efficiency was calculated by dividing the radioactivity of the purified product by the radioactivity of the collected crude product. RCY was defined as the ratio of radioactivity of the purified product to the starting radioactivity on the chip.

To visualize the distribution of radioactivity on the chips, a custom Cerenkov Luminescence Imaging (CLI) setup [28] was used. In particular, we focused on imaging after the collection step. To acquire an image, the chip was placed in a light-tight box, covered with a plastic scintillator (1 mm thick) to increase the luminescence signal, and imaged for 300s. After acquisition, the raw image was processed via image correction and background correction steps as described previously[20]. To analyze the ratio of residual activity within the area of the reaction site to the total residual activity on the chip (i.e., reaction site and surrounding region), regions of interests (ROIs) were drawn to encircle both the reaction site and the whole chip. The desired ratio was calculated as the sum of pixel values within the reaction site ROI divided by sum of pixel values within the whole chip ROI.

3 Results and discussion

3.1 Mock radiosyntheses

To test the feasibility of multi-step reactions on the microdroplet radiosynthesizer, we first performed a mock synthesis of [^{18}F]fallypride, in which [^{18}F]fluoride/$TBAHCO_3$ solution was replaced with DI water, and precursor solution was replaced with the solvent mixture only. Diluted food dyes of different colors were added in each solution: yellow dye was mixed with DI water, red dye was mixed with a mixture of MeCN and thexyl alcohol (1:1, v/v), and blue dye was mixed with a mixture of MeOH and DI water (9:1, v/v). To dispense these solutions, reagent reservoirs were pressurized to ~35 kPa [~5 psi] and an opening

duration of 1.0 ms was used. The synthesis scheme and a series of photographs of the overall process is shown in Figure 4 (see also the Supplemental Video). During the mock synthesis, we observed the rotation stage move the chip quickly and accurately to each desired position, the reagents were accurately delivered to the reaction sites without any visible splashing, and the solutions on the chip remained confined to the reaction site during all steps of the synthesis process.

3.2 [^{18}F]fallypride synthesis

To evaluate the performance and consistency of the [^{18}F]fallypride syntheses, we performed multiple radiosyntheses per day on two separate days (Table 2). Overall, the crude RCY was very high and was consistent across the two days (95 ± 3% (n=5) for day 1 and 97 ± 2% (n=4) for day 2). The fluorination efficiency was very consistent (94.8 ± 0.1% (n=5) for day 1 and 94.3 ± 0.5% (n=4) for day 2), as was the radioactivity recovery (101 ± 3% (n=5) for day 1 and 102 ± 2% (n=4) for day 2). Values greater than 100% are likely a result of slight geometry-related biases that occur in the dose calibrator, e.g. when measuring the activity of a vial versus a chip. Only ~1 % of radioactivity remained stuck to the chip (as unrecoverable activity) on both days.

Notably, the synthesis conditions were taken directly from previous manual efforts to optimize the synthesis of [^{18}F]fallypride [34], with no need for re-optimization. The synthesis performance on the new automated system was very similar to manually-performed syntheses during the optimization studies (Table 3). The similarity is not surprising considering that the high-throughput studies used similar microfluidic chips, but containing a 2×2 array of circular hydrophilic reaction sites (each 4 mm diameter). The fluorination efficiency of the two methods was the same (94.6 ± 0.4% (n=9) for the automated chip, compared to 95 ± 1% (n=6) for the manually-performed high-throughput experiments). However, the radioactivity recovery was higher for the automated setup (101 ± 3% (n=9) versus 91 ± 1% (n=6)). This was due to the improved automated collection process, which eliminated losses due to manual pipetting. Consequently, the crude RCY obtained with the microdroplet reactor was 96 ± 3% (n=9), about ~10% higher than that obtained previously with the high throughput reactor (87 ± 1% (n=6)) [34].

In contrast, the performance of the synthesis on our previous “passive transport” system was substantially lower, with crude RCY of 64 ± 6% (n=4)[20]. However, this previous work was performed using different reaction conditions, making a meaningful comparison of the two technologies impossible. We therefore performed the synthesis on the passive transport chip using the same reaction conditions used in the current paper, and observed a crude RCY of 75 ± 10% (n=5). This result (Table 3) suggests that the design improvements in the new droplet synthesis platform resulted in nearly 30% relative improvement in the RCY, i.e. from 75 ± 10% (n=5) to 96 ± 3% (n=9). By eliminating the hydrophilic reagent delivery “channels”, significant improvements were seen both in the fluorination efficiency as well as recovery efficiency. The increase in fluorination efficiency (i.e. from 81 ± 9% (n=5) to 94.6 ± 0.4% (n=9)) is due to better confinement of both the [^{18}F]fluoride (during the drying step) and precursor (during the radiofluorination step) to the circular reaction site, leading to more uniform concentrations. On our previous passive transport chip, we often saw reagents

slightly spread out along the passive “channels” (i.e. away from the reaction site), leading to unmixed regions and reduced amount of reagents at the actual reaction site. Example radio-TLC chromatograms (in Supplemental Information, Figure S1) confirm that the reaction on the passive transport chip has lower conversion and also has an extra radiolabeled side product. We have observed the amount of this side product to increase when the radio of base to precursor increases, perhaps indicating that there are pockets of abnormally low or high concentrations of reagents during syntheses on the passive transport chip. The circular reaction site also helps to increase the radioactivity recovery (i.e., from 92 ± 5% (n=5) to 101 ± 3% (n=9)), presumably because all of the liquid remains confined to the central reaction region and can more efficiently be collected from the chip. For some experiments, we performed Cerenkov imaging to view the distribution of activity on the chip after collection of the crude product (Figure 5). The residual activity on the circular reaction chip after collection was 0.7 ± 0.3% (n=9) of the starting activity, and 90.6 ± 5.6 % (n=4) of the residual activity was retained within the reaction site (Figure 5A). In contrast, the residual activity on the passive transport chip was significantly higher (7 ± 1% (n=5) of the starting activity), and more than 93% of the residual activity was located on the reagent delivery channels (Figure 5B) where it could not be recovered by the product collection mechanism. Interestingly, the amount of unrecoverable residual activity within the reaction site was similar for both chips (~0.5% for the circular reaction chip vs ~0.4% for the passive transport chip).

By using this new chip design and corresponding apparatus, the crude RCY of [^{18}F]fallypride synthesis was therefore meaningfully augmented.

In addition, the synthesis time was also slightly improved (~17 min here compared to ~20 min in previous work [20]). The fast speed of the rotary actuator limited the amount of time needed to properly position the chip between steps, and the optimized collection procedure (with faster vacuum ramping speed) shaved a few minutes from the overall process time. Further synthesis time reduction may be possible by optimizing the position of dispensers and collection tube within a smaller angular range.

Though the main focus of this work was on developing a new chip and radiosynthesis system for improved and streamlined synthesis steps, we also performed purification of the crude product via analytical radio-HPLC. The purification efficiency was 81% (n=1) and overall RCY was 78% (n=1). Chromatograms of the crude product, purified product and purified product co-injected with fallypride reference standard are shown in Figure 6. Due to the small amount of reagents (i.e. $TBAHCO_3$, precursor) used in microdroplet reactions, the crude product can be purified via analytical-scale HPLC compared to the semi-preparative HPLC used in conventional radiosynthesis. This results in short retention times (and short purification times) and lower mobile phase volume of the collected pure fraction (simplifying and shortening the formulation process). Furthermore, both the UV and radiation detector chromatograms of the crude [^{18}F]fallypride product were in general much cleaner compared to the synthesis carried out in the macroscale [35] (where overlap of product with impurities has been observed). In the radiation detector chromatogram, the product peak was sharp (~0.5 min wide) and well separated from the [^{18}F]fluoride peak and a couple of very small radioactive side-product peaks. In the UV chromatogram, the impurity peaks

were well-defined and were well-separated from the product peak, making separation very straightforward. The needed purification time was only ~5 min (retention time ~4.5 min), and the purified product was 100% radiochemically pure.

4 Conclusions

A very compact (coffee cup-sized) microdroplet radiosynthesizer was developed for performing automated radiochemical reactions. The apparatus (10 × 6 × 12 cm, W x D x H) is over an order of magnitude smaller than commercial synthesizers that are currently considered to be very compact, for example the IBA RadioPharma Solutions Synthera® (17 × 29 × 28.5 cm, W x D x H). Note that in both cases these dimensions include only the apparatus for the core reaction steps; additional equipment is needed to perform purification and formulation processes. Compared to other small-volume reactors listed in Table 1, our platform provides a fully-automated system within a compact space, while other systems require additional, bulky reagent delivery systems or require manual intervention by the radiochemist. The compact size could potentially allow much smaller shielding than a typical hot cell, or could allow a large number of synthesizers to be operated within a single hot cell.

Multi-step chemical reactions (including evaporative drying and radiofluorination) were performed to synthesize the PET tracer [^{18}F]fallypride. The synthesis yield was very high and was consistent within a given day and from day to day. A significant advantage of this next-generation (rotary) platform compared to our previous passive transport approach [20] is that the reaction site (hydrophilic circle) is identical to the shape of the reaction site on chips we use for high-throughput reaction optimization (arrays of circular sites), eliminating the need for any re-optimization.

The small amount of reagents used in the microdroplet reactor resulted in a very clean chromatogram and short retention time (~5 min) despite the purification being performed with only an analytical-scale HPLC column. The small volume of the mobile phase in the collected fraction (~1.5 mL) could be rapidly removed via evaporation for reformulation in saline within ~8 min. This time could potentially be further decreased using a microfluidic-based based PET tracer reformulation device [36].

Recently, we have reported the capability of producing [^{18}F]fallypride at the GBq level by integrating the passive transport based reactor [20] and a micro-cartridge based radionuclide concentrator [33]. In that work, extensive studies were carried out to figure out how to optimally load ~25 μL concentrated [^{18}F]fluoride solution to the small reaction site without having the liquid spread out along the passive transport “channels” which can lead to poor mixing, low reaction efficiencies, and poor recovery of crude product. By integrating the concentrator with the presented next-generation microdroplet radiosynthesizer in the future, it will be much easier and faster to scale up the synthesis to clinically-relevant levels.

In addition to [^{18}F]fallypride, this compact microdroplet reactor can also be used for the synthesis of other PET tracers, such as [^{18}F]FDOPA [31], [^{18}F]FET, and [^{18}F]Florbetaben ([^{18}F]FBB), which we have recently shown can be synthesized in high efficiency in droplet

format, and could also be applied to labeling with other isotopes such as radiometals for both imaging and radiotherapeutic applications. Tools like Cerenkov imaging of chips will likely be helpful during the investigation of other tracers, for example to optimize reagent delivery parameters for new liquids (to prevent splashing of radioactivity outside the reaction site) as described in the Supplemental Information, Section 2.

Other than production of radiopharmaceuticals for imaging or therapy, our automated platform also has the potential to be applied for small scale chemical reactions or assays, in applications where compact apparatus and/or small reagent volumes are critical.

Supplementary Material

Refer to Web version on PubMed Central for supplementary material.

Acknowledgments

We thank Dr. Roger Slavik and the staff of the UCLA Biomedical Cyclotron facility for generously providing [^{18}F]fluoride ion for these studies, and Ksenia Lisova for assisting with HPLC purification. This work was funded in part by the National Institute on Aging (R21 AG049918), the National Cancer Institute (R21 CA212718), and the National Institute of Mental Health (R44 MH097271).

7 References

1. Bergström M, Grahnén A and Långström B, Eur. J. Clin. Pharmacol, 2003, 59, 357–366. [PubMed: 12937873]
2. Matthews PM, Rabiner EA, Passchier J and Gunn RN, Br. J. Clin. Pharmacol, 2012, 73, 175–186. [PubMed: 21838787]
3. Lamberts LE, Williams SP, van Scheltinga AGTT, Hooge MNL, Schröder CP, Gietema JA, Brouwers AH and de Vries EGE, J. Clin. Oncol, 2015, 33, 1491–1504. [PubMed: 25779566]
4. Afshar-Oromieh A, Avtzi E, Giesel FL, Holland-Letz T, Linhart HG, Eder M, Eisenhut M, Boxler S, Hadaschik BA, Kratochwil C, Weichert W, Kopka K, Debus J and Haberkorn U, Eur. J. Nucl. Med. Mol. Imaging, 2015, 42, 197–209. [PubMed: 25411132]
5. Linden HM, Stekhova SA, Link JM, Gralow JR, Livingston RB, Ellis GK, Petra PH, Peterson LM, Schubert EK, Dunnwald LK, Krohn KA and Mankoff DA, J. Clin. Oncol, 2006, 24, 2793–2799. [PubMed: 16682724]
6. Su H, Bodenstein C, Dumont RA, Seimbille Y, Dubinett S, Phelps ME, Herschman H, Czernin J and Weber W, Clin. Cancer Res, 2006, 12, 5659–5667. [PubMed: 17020967]
7. Clark Peter, Ebiana Victoria A., Gosa Laura, Cloughesy Timothy F. and Nathanson David A., J. Nucl. Med, 2017, 58, 689–696. [PubMed: 28385796]
8. Audrain H, Angew. Chem. Int. Ed, 2007, 46, 1772–1775.
9. LU S, CHUN J-H and PIKE VW, J. Label. Compd. Radiopharm, 2010, 53, 234–238.
10. Rensch C, Jackson A, Lindner S, Salvamoser R, Samper V, Riese S, Bartenstein P, Wängler C and Wängler B, Molecules, 2013, 18, 7930–7956. [PubMed: 23884128]
11. Zheng M-Q, Collier L, Bois F, Kelada OJ, Hammond K, Ropchan J, Akula MR, Carlson DJ, Kabalka GW and Huang Y, Nucl. Med. Biol, 2015, 42, 578–584. [PubMed: 25779036]
12. Liang SH, Yokell DL, Normandin MD, Rice PA, Jackson RN, Shoup TM, Brady TJ, El Fakhri G, Collier TL and Vasdev N, Mol. Imaging, 2014, 13, 1–5.
13. Lebedev A, Miraghaie R, Kotta K, Ball CE, Zhang J, Buchsbaum MS, Kolb HC and Elizarov A, Lab. Chip, 2012, 13, 136–145. [PubMed: 23135409]
14. Elizarov AM, van Dam RM, Shin YS, Kolb HC, Padgett HC, Stout D, Shu J, Huang J, Daridon A and Heath JR, J Nucl Med, 2010, 51, 282–287. [PubMed: 20124050]

15. Zhang X, Liu F, Knapp K-A, Nickels ML, Manning HC and Bellan LM, Lab. Chip, 2018, 18, 1369–1377. [PubMed: 29658049]
16. Iwata R, Pascali C, Terasaki K, Ishikawa Y, Furumoto S and Yanai K, J. Label. Compd. Radiopharm, 2018, 61, 540–549.
17. Pascali G, Watts P and Salvadori P, Nucl. Med. Biol, 2013, 40, 776–787. [PubMed: 23684316]
18. Keng PY and van Dam RM, Mol. Imaging, 2015, 14, 579–594.
19. Fiel SA, Yang H, Schaffer P, Weng S, Inkster JAH, Wong MCK and Li PCH, ACS Appl. Mater. Interfaces, 2015, 7, 12923–12929. [PubMed: 26000709]
20. Wang J, Chao PH, Hanet S and van Dam RM, Lab. Chip, 2017, 17, 4342–4355. [PubMed: 29164208]
21. Keng PY, Sergeev M and van Dam RM, in Perspectives on Nuclear Medicine for Molecular Diagnosis and Integrated Therapy, eds. Kuge Y, Shiga T and Tamaki N, Springer Japan, 2016, pp. 93–111.
22. Lisova K, Sergeev M, Evans-Axelsson S, Stuparu AD, Beykan S, Collins J, Jones J, Lassmann M, Herrmann K, Perrin D, Lee JT, Slavik R and van Dam RM, Nucl. Med. Biol, 2018, 61, 36–44. [PubMed: 29747035]
23. Sergeev M, Lazari M, Morgia F, Collins J, Javed MR, Sergeeva O, Jones J, Phelps ME, Lee JT, Keng PY and van Dam RM, Commun. Chem, 2018, 1, 10.
24. Chen S, Javed MR, Kim H-K, Lei J, Lazari M, Shah GJ, van Dam M, Keng PY and Kim C-J, Lab. Chip, 2014, 14, 902–910. [PubMed: 24352530]
25. Lebedev A, in Microfluidic Devices for Biomedical Applications, eds. Li XJ and Zhou Y, Woodhead Publishing, Cambridge, 2013, pp. 594–633.
26. Javed MR, Chen S, Lei J, Collins J, Sergeev M, Kim H-K, Kim C-J, van Dam RM and Keng PY, Chem. Commun, 2014, 50, 1192–1194.
27. Keng PY, Chen S, Ding H, Sadeghi S, Shah GJ, Dooraghi A, Phelps ME, Satyamurthy N, Chatziioannou AF, Kim C-J and van Dam RM, Proc. Natl. Acad. Sci, 2012, 109, 690–695. [PubMed: 22210110]
28. Dooraghi AA, Keng PY, Chen S, Javed MR, Kim C-J“CJ”, Chatziioannou AF and van Dam RM, Analyst, 2013, 138, 5654–5664. [PubMed: 23928799]
29. Javed MR, Chen S, Kim H-K, Wei L, Czernin J, Kim C-J“CJ”, van Dam RM and Keng PY, J. Nucl. Med, 2014, 55, 321–328. [PubMed: 24365651]
30. Bejot R, Elizarov AM, Ball E, Zhang J, Miraghaie R, Kolb HC and Gouverneur V, J. Label. Compd. Radiopharm, 2011, 54, 117–122.
31. Wang J, Holloway T and Van Dam RM, Eur. J. Nucl. Med. Mol. Imaging, 2018, 45(Suppl 1), S662.
32. Chao PH, Lazari M, Hanet S, Narayanam MK, Murphy JM and van Dam RM, Appl. Radiat. Isot, 2018, 141, 138–148. [PubMed: 30243135]
33. Chao PH, Wang J and Van Dam RM, in Proceedings of the 22nd International Conference on Miniaturized Systems for Chemistry and Life Sciences, Royal Society of Chemistry, Kaohsiung, Taiwan, 2018, pp. 1155–1158.
34. Rios A, Wang J, Chao PH and Van Dam RM, in Proceedings of the 22nd International Conference on Miniaturized Systems for Chemistry and Life Sciences, Royal Society of Chemistry, Kaohsiung, Taiwan, 2018, pp. 1065–1067.
35. Seok Moon B, Hyung Park J, Jin Lee H, Sun Kim J, Sup Kil H, Se Lee B, Yoon Chi D, Chul Lee B, Kyeong Kim Y and Eun Kim S, Appl. Radiat. Isot, 2010, 68, 2279–2284. [PubMed: 20609592]
36. Chao PH, Collins J, Argus JP, Tseng W-Y, Lee JT and van Dam RM, Lab. Chip, 2017, 17, 1802–1816. [PubMed: 28443841]
37. Matesic L, Kallinen A, Greguric I and Pascali G, Nucl. Med. Biol, 2017, 52, 24–31. [PubMed: 28599133]
38. Lazari M, Collins J, Shen B, Farhoud M, Yeh D, Maraglia B, Chin FT, Nathanson DA, Moore M and van Dam RM, J. Nucl. Med. Technol, 2014, 42, 203–210. [PubMed: 25033883]
39. Kramer V, Piel M, Elgueta C, Höhnemann S, Amaral A, Avila-Sobarzo M, Ribbeck J, Perez E, Rösch F and Amaral H, J. Nucl. Med, 2013, 54, 1014–1014. [PubMed: 23651946]

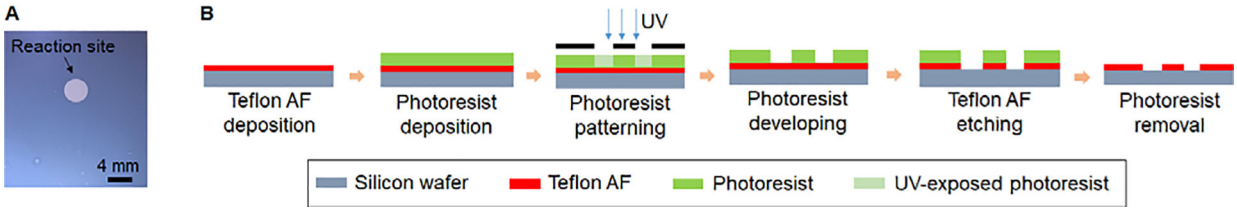

Figure 1.

(A) Photo of the microfluidic chip. Diameter of the hydrophilic reaction site is 4 mm. (B) Photolithography process for fabrication of the microfluidic chip.

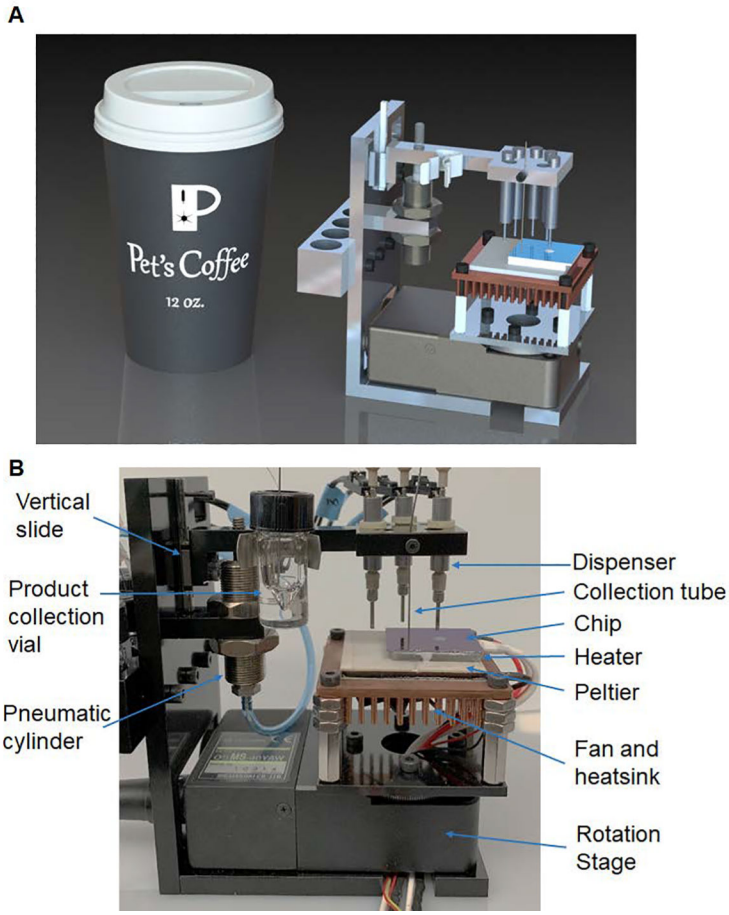

Figure 2.

The microdroplet radiosynthesizer. (A) A CAD rendering of the system alongside a 12 oz. coffee cup. (B) A photograph of the synthesizer, including the reagent dispensing, product collection, temperature control, and rotation subsystems.

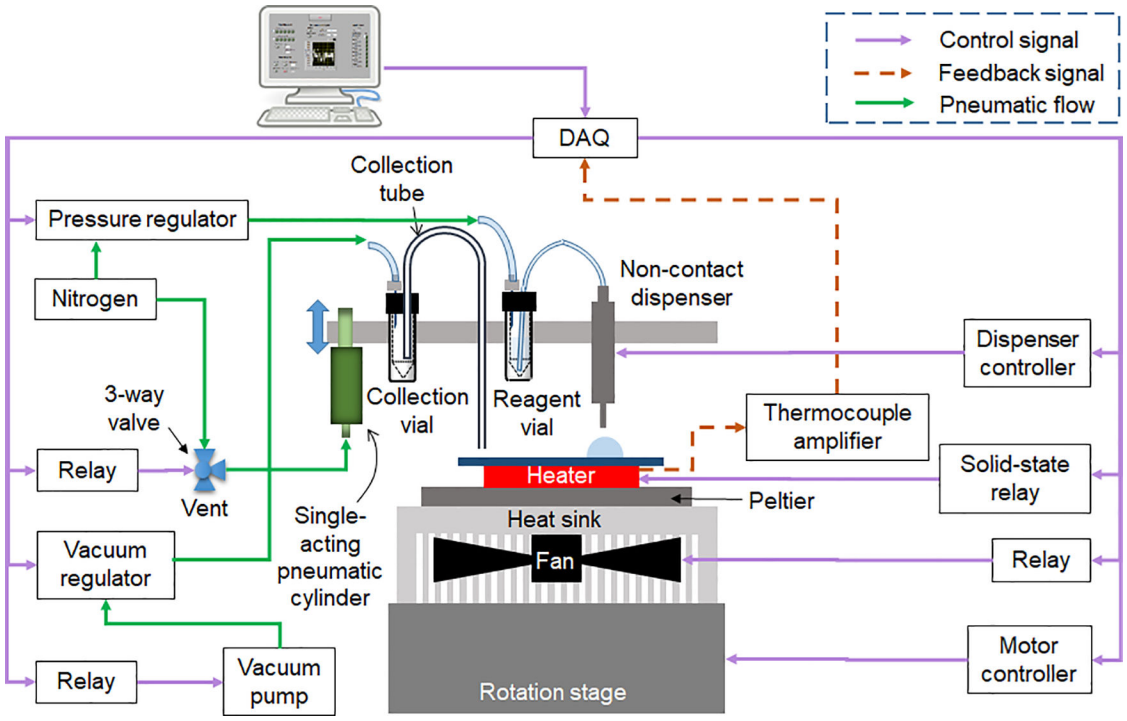

Figure 3.
Control system of the microdroplet radiosynthesizer.

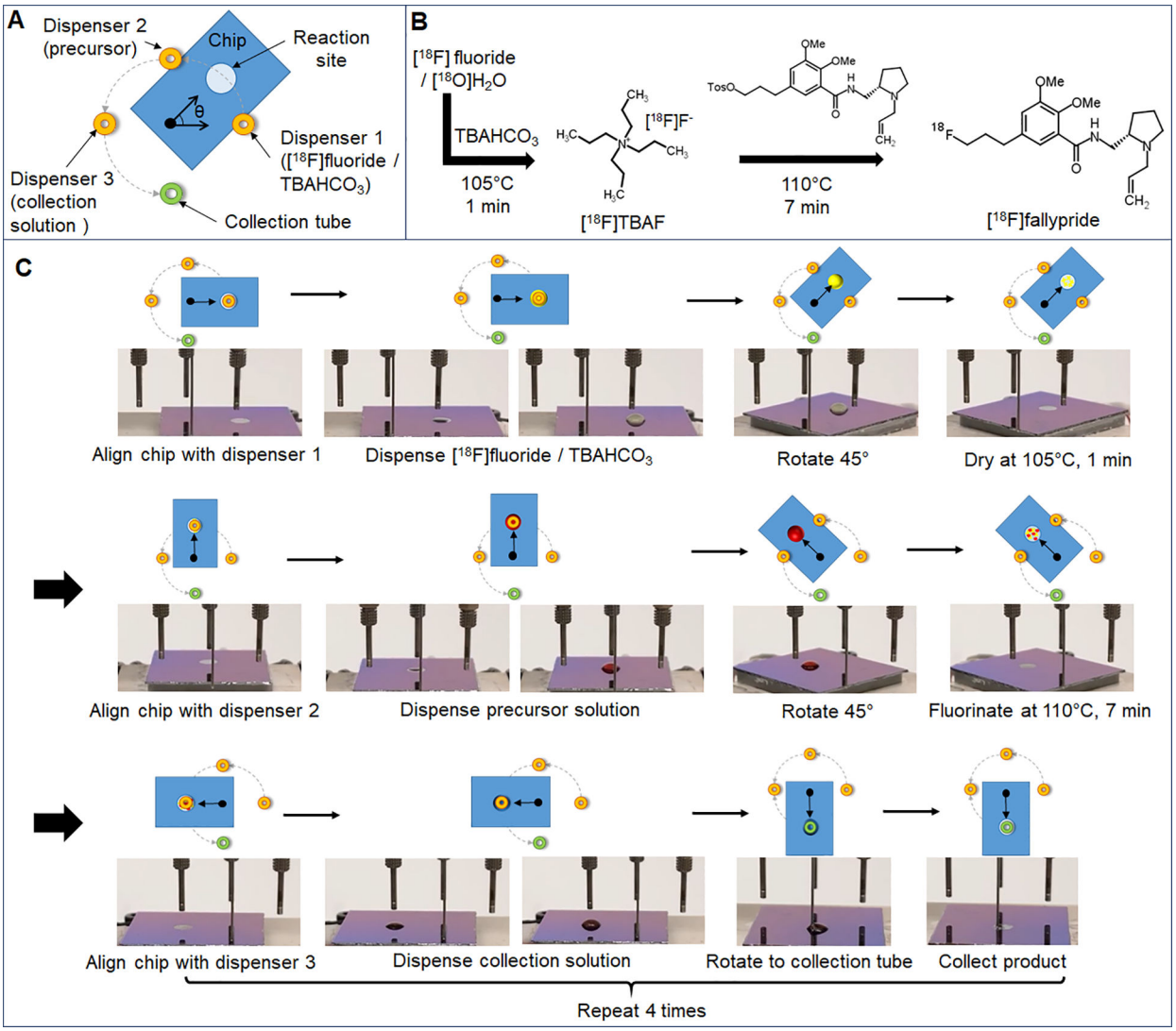

Figure 4.

(A) Top view schematic of the (moveable) microfluidic chip and (fixed) locations of reagent dispensers and the collection tube. The angle marker shows the center of rotation. (B) Synthesis scheme. (C) Schematic (showing chip orientation) and photograph of the chip (using mock reagents) for each step of the [^{18}F]fallypride synthesis process. First the chip was rotated under the [^{18}F]fluoride/TBAHCO$_3$ dispenser and 10 droplets (1μL each; DI water, dyed yellow) were loaded at the reaction site. Then, the chip was rotated 45° and heated to 105°C to remove the solvent. Next, the chip was rotated 45° under the precursor dispenser, 10 droplets (1μL each; 1:1 v/v MeCN/ thexyl alcohol, dyed red) were loaded, and then the chip was rotated 45° and heated to 110°C to simulate the fluorination reaction. Next, the chip was rotated 45° under the collection solution dispenser and 20 droplets (1μL each; 9:1 v/v MeOH/water, dyed blue) were loaded to dilute the reaction mixture. Finally the chip was rotated 90° under the collection tube, and the droplet was collected into the product vial using vacuum. The collection solution loading and collecting were repeated a total of 4 times to minimize the residue left behind at the reaction site.

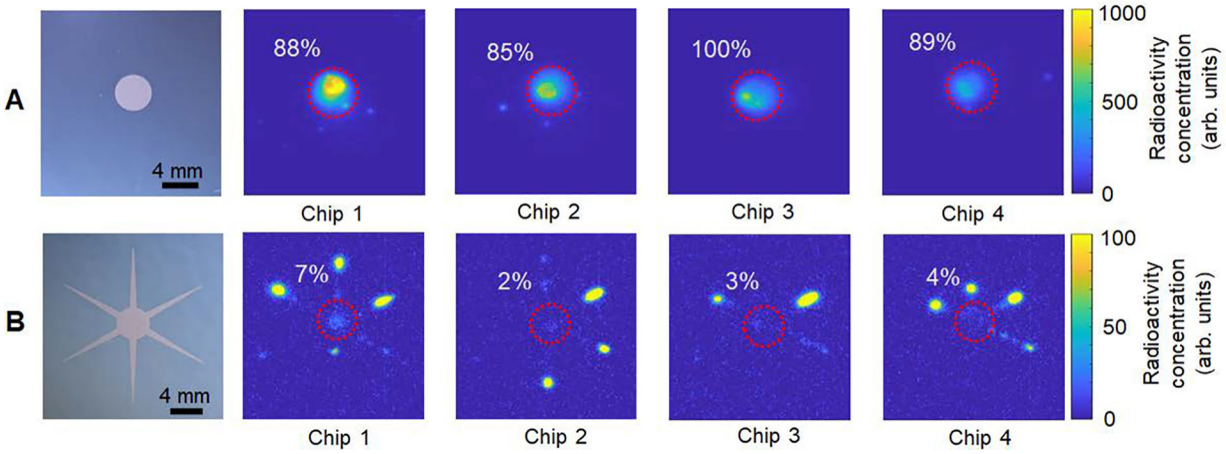

Figure 5.

Activity distribution on (A) the circular pattern chip and (B) the passive transport chip after collection of the crude product, visualized with Cerenkov luminescence imaging. Four example images are shown for each case. The red dashed circle marks the reaction site and the numerical value indicates the fraction of total residual activity on the chip that is present inside the reaction site.

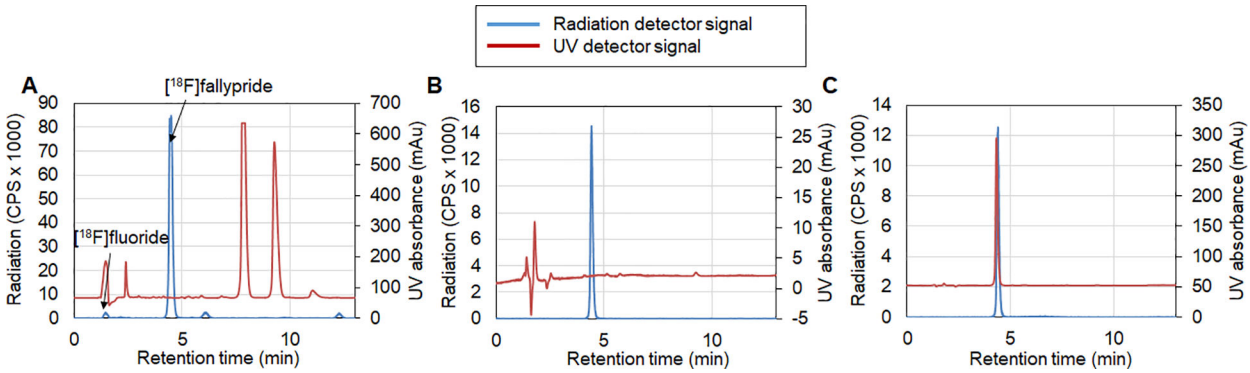

Figure 6.

HPLC chromatograms of (A) crude [^{18}F]fallypride, (B) purified [^{18}F]fallypride, and (C) purified [^{18}F]fallypride co-injected with fallypride reference standard for identity verification. Radiochemical purity was 100%.

Table 1.

Comparison of various radiosynthesizers (both microscale and macroscale) that have been used for the synthesis of [^{18}F]fallypride. Total synthesis time includes purification and formulation. Total system size include all hardware requiring shielding that is needed to perform synthesis (not including purification and formulation). All RCY values are decay corrected. Where applicable, values are expressed as average ± standard deviation, computed from the indicated number of measurements.

	Reference	Reaction volume (μL)	Precursor amount (nmol)	Total synthesis time(min)	RCY (%)	Reaction mode	Commercialized?	Automation
This work		6	231	30	78 (n=1)	Batch	No	Full
UCLA EWOD chip	Javed et al.[26]	4	308	60	65±6 (n=7)	Batch	No	Semi[a]
Tohoku Microvolume in Glass vial	Iwata et al.[16]	20	80	N.A.	47±10 (n=?)	Batch	No	Manual
Siemens Microreactor assembly	Lebedev et al.[13]	50	1936	45	37±5 (n=?)	Batch	No	Full
Vanderbilt PDMS chip	Zhang et al.[15]	100	5807	60	10 ± 3 (n=?)	Batch	No	Semi[b]
Advion NanoTek	Matesic et al.[37]	100	387 (in 100 μL)[c]	55±3 (n = 9)	25±13 (n=9)	Flow	Yes	Full
GE TracerLab FXFN	Moon et al.[35]	1000	3872	51±1.2 (n = 42)	68±1.6 (n=42)	Batch	Yes	Full
Sofie ELIXYS	Lazari et al.[38]	1000	7744	56+formulation	66±8 (n=6)	Batch	Yes	Full
IBA Synthera	Kramer et al.[39]	N.R.	N.R.	55–65	36 (n=?)	Batch	Yes	Full

N.R. indicates not reported.

[a] In the EWOD chip, droplet manipulation and temperature control are performed automatically, but loading of reagent droplets and collection of crude product are performed manually via pipette.

[b] In the Vanderbilt PDMS reactor, fluid is automatically loaded into the chip via syringe pump, but manual activation of numerous components (switching valve states, opening evaporation vent in reactor, switching reagent connections, and hot plate heating) is needed.

[c] In flow-through reactions such as the Advion NanoTek, scaling up to higher activity levels will increase the amount of precursor consumed.

[d] To synthesize [^{18}F]fallypride, three different modules would be needed, i.e. a drying module, a syringe pump module and a capillary reactor module. But we couldn't locate the information about the size of those modules in any literature or brochures.

Table 2.

Comparison of [^{18}F]fallypride syntheses performed on different days. Synthesis time for all experiments was ~17 min. All measurements are decay corrected. All values are average ± standard deviation, computed from the indicated number of measurements on each day.

	Day 1 (N=5)	Day 2 (N=4)
Radioactivity recovery (%)	101 ± 3	102 ± 2
Fluorination efficiency (%)	94.8 ± 0.1	94.3 ± 0.5
Crude RCY (%)	95 ± 3	97 ± 2
Residual activity on chip (%)	0.7 ± 0.4	0.8 ± 0.2

Table 3.

Comparison of [^{18}F]fallypride syntheses performed on the new automated droplet synthesis platform (circular reaction site), high-throughput chips (containing 2×2 array of circular reaction sites) and the previous automated passive transport reactor (single reaction site with six tapered droplet transport channels). The same reaction conditions were used in all cases. All measurements are decay corrected. All values are average ± standard deviation, computed from the indicated number of measurements in each case.

	Automated operation on single-reaction chip	Manual operation on high-throughput chip	Passive transport reactor
Number of experiments	9	6	5
Radioactivity recovery (%)	101 ± 3	91 ± 1	92 ± 5
Fluorination efficiency (%)	94.6 ± 0.4	95 ± 1	81 ± 9
Crude RCY (%)	96 ± 3	87 ± 1	75 ± 10
Residual activity on chip (%)	0.7 ± 0.3	0.12 ± 0.05	7 ± 1
Residual activity on the reaction site (%)	0.5 ± 0.3 (n=4)	NA	0.4 ± 0.2